Repository of Hochschule Hannover

HOCHSCHULE
HANNOVER
UNIVERSITY OF
APPLIED SCIENCES
AND ARTS

Diffusion of hydrogen into and through γ-iron by density functional theory

Urslaan Chohan, Sven P. K. Köhler, Enrique Jimenez-Melero

Suggested citation:

Chohan, Urslaan, Sven P. K. Köhler, and Enrique Jimenez-Melero. 2018. "Diffusion of hydrogen into and through γ-iron by density functional theory." *Surface Science* 672-673: 56–61. https://doi.org/10.25968/opus-2272.

Abstract

This study is concerned with the early stages of hydrogen embrittlement on an atomistic scale. We employed density functional theory to investigate hydrogen diffusion through the (100), (110) and (111) surfaces of γ-Fe. The preferred adsorption sites and respective energies for hydrogen adsorption were established for each plane, as well as a minimum energy pathway for diffusion. The H atoms adsorb on the (100), (110) and (111) surfaces with energies of −4.06 eV, −3.92 eV and −4.05 eV, respectively. The barriers for bulk-like diffusion for the (100), (110) and (111) surfaces are −0.6 eV, −0.5 eV and −0.7 eV, respectively. We compared these calculated barriers with previously obtained experimental data in an Arrhenius plot, which indicates good agreement between experimentally measured and theoretically predicted activation energies. Texturing austenitic steels such that the (111) surfaces of grains are preferentially exposed at the cleavage planes may be a possibility to reduce hydrogen embrittlement.

Terms of use

CC BY-NC-ND 4.0

This document is made available under these conditions:
Creative Commons - CC BY-NC-ND - Namensnennung - Nicht kommerziell - Keine Bearbeitungen 4.0 International
For more information see:
https://creativecommons.org/licenses/by-nc-nd/4.0/deed.de

Diffusion of Hydrogen into and through *γ*-Iron by Density Functional Theory

Urslaan K. Chohan [a,*], *Sven P. K. Koehler*[b,c], *Enrique Jimenez-Melero*[a]

[a]School of Materials, The University of Manchester, Manchester M13 9PL, UK

[b]School of Science and the Environment, Manchester Metropolitan University, Manchester M1 5GD, UK

[c]Photon Science Institute, The University of Manchester, Manchester M13 9PL, UK

*Corresponding author.

Email: urslaan.chohan@postgrad.manchester.ac.uk

University of Manchester

School of Materials

Oxford Road

Manchester

M13 9PL

United Kingdom

Abstract

This study is concerned with the early stages of hydrogen embrittlement on an atomistic scale. We employed density functional theory to investigate hydrogen diffusion through the (100), (110) and (111) surfaces of γ-Fe. The preferred adsorption sites and respective energies for hydrogen adsorption were established for each plane, as well as a minimum energy pathway for diffusion. The H atoms adsorb on the (100), (110) and (111) surfaces with energies of ~4.06 eV, ~3.92 eV and ~4.05 eV, respectively. The barriers for bulk-like diffusion for the (100), (110) and (111) surfaces are ~0.6 eV, ~0.5 eV and ~0.7 eV, respectively. We compared these calculated barriers with previously obtained experimental data in an Arrhenius plot, which indicates good agreement between experimentally measured and theoretically predicted activation energies. Texturing austenitic steels such that the (111) surfaces of grains are preferentially exposed at the cleavage planes may be a possibility to reduce hydrogen embrittlement.

Keywords: gamma iron, hydrogen embrittlement, hydrogen diffusion, potential energy surface, surface relaxation, density functional theory

1. Introduction

Hydrogen embrittlement (HE) is a process critical to the degradation of materials and structures, as it affects the integrity of a range of engineering materials such as advanced steels [1, 2] and nickel-based alloys [3, 4]. The HE process can lead to premature environmentally-assisted failure in those structures, which can have catastrophic consequences across a range of practical applications such as in the nuclear industry and steel oil/gas pipelines. The cost of material failure can be significant, such as the failure of steel bolts due to HE in a single high-rise office block, costing over £6M [5]. In the HE process, hydrogen enters the bulk structure of metals via diffusion, which leads to the gradual accumulation of hydrogen and a resulting increase in the brittleness of the material. There are two principal mechanisms proposed for the HE phenomenon, namely the HELP (Hydrogen Enhanced Localised Plasticity) and HEDE (Hydrogen Enhanced DEcohesion) mechanisms. In HELP, hydrogen lowers the activation energy for dislocation motion and facilitates the formation of highly-deformed localised regions in the microstructure, which allows the rapid initiation and propagation of a crack tip [6, 7]. In HEDE, the hydrogen reduces the interatomic cohesive forces and favours the cleavage of planes along grain boundaries [8, 9].

The diffusion of hydrogen into metal surfaces occurs sequentially. In the initial step, hydrogen molecules physisorb onto the exposed metallic surface [10, 11]. In the next stage, the hydrogen molecule dissociates into hydrogen atoms. This process occurs readily on transition metal surfaces, with a low (or no) energy barrier for dissociation - due to the interaction between H_2 bonding electrons and the d-electron holes in the metal surface [11]. Additionally, at low temperatures these processes are strongly enhanced due to increasing collision rates [12], therefore hydrogen molecules readily physisorb and dissociate into hydrogen atoms at low temperatures. Prior to hydrogen atoms entering the bulk structure, they typically adsorb at specific lowest energy sites above the surface. The hydrogen atoms

may recombine to form molecular hydrogen at this stage, which is surface diffusion driven process. However, the surface diffusion rate is ~10^{-3} times slower than the bulk diffusion rate, with similar activation energies, hence the overall process is dominated by bulk diffusion [13]. They can subsequently diffuse into the bulk, and are likely to travel on or close to the minimum energy path (MEP), depending on the available energy. In this work, we investigated the hydrogen adsorption and sub-surface diffusion through the (100), (110) and (111) surfaces of the face-centred cubic (fcc) phase of iron, namely γ-Fe. This phase is the base of austenitic steels used in nuclear reactor applications [14, 15], especially in the pipelines of fission reactors [16], and also of (ultra-)high strength steels for the automotive industry [17-20]. The γ-phase of Fe is stable in the range of temperatures of 1185-1665 K [21], but can be present in microstructures in a metastable condition at lower temperatures by adding γ-stabilising alloying elements such as nickel, manganese, carbon or nitrogen [20, 22]. Most of the previous work focuses on hydrogen diffusion through bulk γ-Fe and along defects such as dislocation lines [23], stacking faults [24] and grain boundaries [25]. Relatively deep hydrogen traps in the steel microstructure are already saturated at low values of hydrogen activity and do not affect the hydrogen diffusivity significantly [26]. Also, the majority of the past studies concerned with hydrogen diffusion on and through iron focus on the body-centred cubic α-phase [27-30]. Hydrogen solubility at room temperature is approximately three orders of magnitude higher in fcc steels, but H bulk diffusivity is significantly lower, as compared to bcc steels [23, 31].

Density functional theory (DFT) has previously been shown to efficiently model diffusion of hydrogen into subsurface [32-34] and through bulk [35] of metals, which is critical in the HE process [26]; therefore, we have chosen to apply DFT to model hydrogen diffusion in γ-Fe to elucidate the early stages of HE in this phase relevant to austenitic steels. The investigation of the potential energy surface (PES) that governs diffusion provides

critical insight into the energetics of the process [36] and affords a detailed understanding of the on-surface adsorption and sub-surface diffusion process through γ-Fe. A PES is a multidimensional map of the energy of a chemical system as a function of the degrees of freedom in that system. Higher-dimensional PESs become increasingly difficult to represent graphically. However, an insight into any process can be derived by limiting the degrees of freedom that are considered. In the diffusion process treated here, this entails tracing the energy of a hydrogen atom diffusing through the Fe slab as a function of the x and y coordinates, as well as the depth within the slab, i.e. below the surface. To calculate the PES for the present process, the energy of a single H atom is calculated at a number of points on a regularly-spaced 3D grid of the Fe slab, beginning with a plane above the surface, and inwards towards the bulk. At each depth, a 2D (reduced-dimensionality) PES is generated from the DFT calculations, yielding the minimum energy site towards which the hydrogen atom would preferentially move within that plane. Above the surface, the 2D map yields the preferential site for H atom adsorption. Connecting each minimum energy point along the slab for each 2D map approximates a MEP for H diffusion from the surface into the bulk.

2. Computational Methods

The potential energy surfaces for hydrogen adsorption on the surface and diffusion into sub-surfaces of γ-Fe were calculated for the (100), (110) and (111) surfaces, using density functional theory (DFT) implemented in the Vienna *ab initio* simulation package (VASP) [37]. We used a plane-wave basis set and 3D periodic boundary conditions to describe electronic interactions. The exchange and correlation effects were included using the generalised-gradient approximation (GGA), via the Perdew-Burke-Erzenhof (PBE) functional [38]. The projector augmented-wave (PAW) approximation describes the interaction between the ionic core and valence electrons [39].

A seven Fe layer slab model was used to model surfaces and bulk of γ-Fe. The lattice parameter, a, for γ-Fe was calculated to be 3.43 Å, which is in reasonable agreement with previous calculations (3.45 Å [40-42], 3.49 Å [43]) and the experimental value of 3.56 Å [44]. A (2×2) cell was applied in all calculations. A cutoff energy of 400 eV and a vacuum spacing of 20 Å were found to sufficiently converge the total energy of the system. The Monkhorst-Pack algorithm [45] was used with a grid size of 7×7×1 for the (100), (110) and (111) surfaces. The Methfessel Paxton method of order $N = 1$ with width 0.1 eV was used to apply electronic smearing [46]. The slabs were minimised using the conjugate gradient method [47], until forces were within 10^{-5} eV/Å. The three bottom layers were ionically constrained. The energies of all atoms were converged to within 10^{-6} eV.

A mesh grid was used to sample various hydrogen positions within the slab. A large number of points was used to create a tight mesh, which would accurately describe the potential energy surface. The mesh consisted of a 6×6 uniform grid in the x-y plane parallel to the surface, sampling only a quarter of the surface unit cell due to symmetry considerations, i.e. sampling on the domain $x,y \in [0,0.5]$, in fractional coordinates; however, this domain was expanded by appropriate mirroring to yield 144 points on the surface unit cell. An equivalent 2D mesh was applied at nine selected positions along the z direction of the slab (i.e. into the bulk): four meshes at the first four Fe layers, three further meshes centrally located in between these Fe layers, and finally two meshes above the surface to simulate H adsorption. The mesh is illustrated in Figure 1a-c for each surface. For each point of the mesh, a single H atom was placed, with the z coordinate constrained, and the energy of the slab was minimised by allowing all Fe atoms in the first four layers to relax. The energies at each point, E, were calculated via the relation

$$E = E_{\text{slab+H}} - (E_{\text{slab}} + E_{\text{H}}) \quad (1)$$

where $E_{\mathrm{slab+H}}$ is the energy of the slab with H incorporated, E_{slab} is the energy of the H-free slab and E_{H} is the ground state energy of a single free H atom in a 10 × 10 × 10 Å^3 box. The energies were then calculated relative to the global minimum of the entire slab, which was set to zero energy.

3. Results and Discussion

3.1 Surface hydrogen adsorption

The adsorption of hydrogen on the (100), (110) and (111) surfaces of γ-Fe was investigated to find the preferred site of adsorption in each case, see Figure 1d-f. A 6 × 6 mesh grid was placed above each surface and the energy was minimised at each point. The adsorption energy was then calculated using Eq. 1. The results are collected in Table 1. For the (100) surface, it was found that the H prefers to reside at the fourfold (4f) site, where the Fe atoms are equidistant to one another, with an adsorption energy of 4.06 eV per H atom relative to a free H atom. For the (110) surface, the H atom prefers to reside at the short-bridge (sb) site, which is the shortest distance between two Fe atoms, with an adsorption energy of 3.92 eV per H atom. On the (111) surface, the H atom prefers to adsorb on the three-fold (3f) site, which, similar to the (100) surface, is the point where the Fe atoms are equidistant from one another; the corresponding adsorption energy is 4.05 eV per H atom. Thus, H atoms bind most tightly to the (100) surface, however the energies are very close to one another between all three surfaces, with only a 0.01 eV difference between the (100) and (111) surfaces. More importantly, for a polycrystalline sample of γ-Fe, this means that H is almost equally likely to adsorb no matter which surface is exposed, i.e. the initial step of HE, the adsorption of H to the surface, is almost independent of the grain orientation or crystallographic texture of the material.

3.2 Subsurface hydrogen diffusion

The process of diffusion from the surface to the sub-surfaces was modelled by investigating the potential energy surface of the whole slab. The relative minimum energies for the H atom in each sampled depth of the (100), (110) and (111) surfaces are collected in Table 1. For each surface, the MEP for diffusion was found by connecting the (energy) minima at each of the nine sampled depths. A reduced cell was considered for sampling, as illustrated in Figs. 2(c), 3(c) and 4(c), because of symmetry considerations. Important subsurface sites such as the octahedral and tetrahedral sites were sampled using the mesh method for each surface.

The 2D potential energy surfaces at selected depths in the Fe slabs are shown in Fig. 2-4 for the (100), (110) and (111) surfaces respectively, together with the minima at each of the calculated mesh depths to represent the minimum energy path for H subsurface diffusion. For all three surfaces considered, it was found that an energy barrier needs to be overcome in order for the hydrogen atom to penetrate the γ-Fe slab. This barrier is ~1.4 eV for the (100) surface, ~1.2 eV for the (110) surface and ~1.7 eV for the (111) surface, see Figures 2(b), 3(b), and 4(b). Therefore, most energy is required to drive the hydrogen into the (111) surface; this has deeper implications, namely that a first consideration for preventing HE would be to consider producing a textured polycrystalline austenitic steel in which most of the surface grains are oriented such that their (111) surface is exposed to the hydrogen containing environment [48].

The H trajectory for diffusion perpendicular to the three surfaces does not follow a linear path into the bulk, but instead the hydrogen diffuses to sub-surface sites along certain pathways, moving between local maxima and minima, see Figures 2, 3, and 4, (b) and (c), respectively. For the (100) surface, we found that the local minima are located in the plane of Fe atoms for all sub-surfaces, and these local minima are located at the octahedral sites. Similarly, for the (110) surface, there are local minima in each of the sub-surface planes

containing Fe atoms; these local minima are at the high-symmetry sites, namely alternatively the long and short-bridge sites. Due to the non-orthogonal unit cell structure for the (111) surface and the ABCABC packing structure, the trajectory and respective energetics for the (111) surface are most complex. In contrast to the (100) and (110) surfaces, however, we observe the local minima for the H atoms to be in-between the close-packed planes containing Fe atoms, and the local maxima in the planes containing Fe atoms.

We have hence calculated the MEP of hydrogen atoms moving from the surface into the bulk, and can estimate from the local minima and maxima the barriers for absorption of the H from the surface into the bulk, and the barriers for diffusion from one sub-surface layer to the next. The activation energies, E_a, obtained from the data shown in Fig. 2-4 can then be compared to the reported experimental values of the diffusion energies of H in austenitic steels. The temperature dependence of the diffusion coefficient (D) for thermally-activated H diffusion can be expressed by the Arrhenius-type equation

$$D = D_0 \exp\left(-\frac{E_a}{kT}\right) \quad (2)$$

where D_0 is the pre-exponential factor (in $m^2\ s^{-1}$), k is the Boltzmann constant (in $eV\ K^{-1}$) and T the temperature (in K). Fig. 5 shows ln D plotted against $1/T$. We compared the activation energies obtained in our calculations with those measured in austenitic stainless steels; these typically contain alloying elements, of course, while we investigated pure γ-Fe. A series of experimental investigations of the diffusivity of hydrogen through austenitic stainless steels and pure γ-Fe were compared by Oriani et al. [49]. It was found that pure γ-Fe has an activation energy of ~0.5 eV, which is close to the activation energy of austenitic stainless steels. Further to this, our simulation box contained 28 Fe atoms only, but we only followed the MEP through the first ten Fe atoms, hence a 10% alloy would only replace one Fe atom on average, and we hereby make the assumption that low-concentration alloying

elements would only have a small counteracting effect on the overall energetics of diffusion [50, 51]. However, we stress that this is an approximation only, especially in nitrogen-containing austenitic steels since this interstitial element can act as an effective trap for hydrogen [51]. Moreover, weak hydrogen trapping in the structure does not change the temperature dependence of the diffusivity in austenitic stainless steels, as it does in iron-based bcc alloys [49]. It was found that in the experiments, using a range of techniques such as thermal desorption and hydrogen permeation testing, E_a for bulk H diffusion in austenitic steels was ~0.5 – 0.7 eV [52-60]. In our investigation, we calculated two activation energies, namely the total activation energy and the bulk-like activation energy for diffusion. The total activation energies were ~1.4 eV for the (100) surface, ~1.2 eV for the (110) surface and ~1.7 eV for the (111) surface, whilst the bulk-like activation energies were ~0.6, 0.5 and 0.7 eV for the (100), (110) and (111) surfaces, respectively. Whilst the total energy barrier is approximately twice the barrier as measured in the experiments, the bulk-like activation energy fits the experimental values closely. These activation energies indicate that it takes a relatively large amount of energy to initially embed the hydrogen into each given surface, whilst bulk diffusion requires relatively less energy. The experiments measured the energies for the diffusion of hydrogen through the bulk, and these match our calculated bulk-like diffusion barriers rather well. It is worth noting that the activation energies for all three surfaces are quite close in the bulk-like region, with the (110) surface having the lowest activation energy. Thus the hydrogen may have a particular preference for following a diffusion pathway perpendicular to the (110) plane in a polycrystalline system. However it is possible that the hydrogen may also penetrate via the other surfaces, if the H can overcome the larger total barrier related to the (100) and (111) surfaces.

In our calculations, we have neglected quantum tunnelling effects between available adjacent interstitial sites, which are important to consider for an H atom diffusing in any

system, given the low mass of hydrogen [61]. Incorporating tunnelling would result in a larger diffusion coefficient, since it implies diffusion without H overcoming an energy barrier. However, whereas the magnitude of tunnelling would stay constant, its contribution to the overall diffusion coefficient would decrease at increasing temperatures as classical trajectories over the barrier dominate [62-64]. Furthermore, it is worth noting that the real energy profile is highly complex, consisting of multiple dimensions. This could mean that a reaction coordinate that is not considered has a significant influence on the energy profile. To give an example: we allowed the Fe atoms to relax for every H atom position from otherwise identical starting configurations; the obtained local minima have no memory of the previous lowest energy configuration, it is hence possible that the Fe atoms have moved considerably while the next H atom position is close to the previous one. Nevertheless, the overall agreement between our values and experimental values from literature shows that our methodology produces a reasonably good approximation of the energy barrier for H diffusion, and delivers a diffusion trajectory through bulk Fe. While adsorption to the three different γ-Fe surfaces considered is energetically similar, the energy barrier for diffusion is highest for the (111) surface, especially through the first Fe layers close to the surface, such that diffusion could be limited even in a polycrystalline textured sample whose (111)-oriented grains are preferentially exposed to the hydrogen-containing environment.

4. Conclusions

In this study, we applied density functional theory to investigate hydrogen diffusion through the three major planes in γ-Fe, namely the (100), (110) and (111) surfaces. This study is relevant for a mechanistic understanding of critical stages of hydrogen embrittlement in austenitic steels, namely the adsorption and sub-surface diffusion towards the bulk structure. The adsorption sites for H on the surface were found for each given plane, along with the adsorption energy. A minimum energy pathway for diffusion was approximated by

conducting a series of energy minimisations, where H atoms were placed in a 6×6 mesh and at nine depths along the slab, starting from above the surface and including the fourth layer. It was found that for the (100) surface, the H atom preferentially adsorbs at the fourfold site, with an adsorption energy of ~4.06 eV. On the (110) surface, the H atom prefers to adsorb at the short-bridge site, with an adsorption energy of ~3.92 eV. Finally, on the (111) surface, the H atom prefers to reside at the threefold site, with an adsorption energy of ~4.05 eV. Thus, the H atom is most tightly bound to the (100) and the (111) surface. For the (100) surface, there is a ~0.6 eV barrier for bulk-like diffusion into the sub-surfaces, whilst for the (110) surface there is a ~0.5 eV barrier for bulk-like diffusion into the sub-surfaces. For the (111) surface, there is a barrier of ~0.7 eV. These barriers are in good agreement with experimental data about bulk H diffusion in these materials, which is shown via Arrhenius plots comparing our calculated and previous experimental data. It appears that one way to reduce hydrogen embrittlement in γ-Fe would be to produce textured austenitic materials with the (111) surface exposed.

Acknowledgements

We would like to thank the Engineering and Physical Sciences Research Council UK (EPSRC) through the Centre for Doctoral Training in Advanced Metallic Systems for the financial support (EP/L016273/1). We gratefully acknowledge the Dalton Cumbrian Facility, partly funded by the Nuclear Decommissioning Authority (NDA), for providing funding to cover the cost of computational time.

References

[1] Konno, R., Manabe, T., Matsui, N., Hirakami, D. and Takai, K. (2017) Factors Causing Hydrogen Embrittlement of Cold-Drawn Pearlitic Steel Fractured Under Elastic/Plastic Region. In TMS (ed), *TMS 2017 146th Annual Meeting and Exhibition Supplemental Proceedings*. Springer International Publishing.

[2] Jemblie, L., Olden, V. and Akselsen, O. M. (2017) A coupled diffusion and cohesive zone modelling approach for numerically assessing hydrogen embrittlement of steel structures. *Int. J. Hydrogen Energy*. **42**(16) 11980-11995.

[3] Klapper, H. S., Klöwer, J. and Gosheva, O. (2017) Hydrogen embrittlement: the game changing factor in the applicability of nickel alloys in oilfield technology. *Phil. Trans. R. Soc. A*. **375**(2098) 20160415(1)-20160415(10).

[4] Tehranchi, A. and Curtin, W. A. (2017) Atomistic study of hydrogen embrittlement of grain boundaries in nickel: I. Fracture. *J. Mech. Phys. Solids*. **101** 150-165.

[5] Tovey, A. (2015) Cheesegrater bolt failures to cost Severfield £6m. The Telegraph.

[6] Birnbaum, H. K. and Sofronis, P. (1994) Hydrogen-enhanced localized plasticity - a mechanism for hydrogen-related fracture. *Mater. Sci. Eng. A* 191-202.

[7] Abraham, D. P., Altstetter, C.J. (1995) Hydrogen-enhanced localization of plasticity in an austenitic stainless steel. *Metall. Trans. A*. **26**(A) 2859-2871.

[8] Troiano, A. R. (1960) The role of hydrogen and other interstitials on the mechanical behavior of metals. *Trans. Am. Soc. Met.* **52** 54-80.

[9] Oriani, R. A. (1978) Hydrogen embrittlement of steels. *Annu. Rev. Mat. Sci.* . **8**(1) 327-357.

[10] Martin, M., Weber, S., Izawa, C., Wagner, S., Pundt, A. and Theisen, W. (2011) Influence of machining-induced martensite on hydrogen-assisted fracture of AISI type 304 austenitic stainless steel. *Int. J. Hydrog. Energy*. **36**(17) 11195-11206.

[11] Christmann, K. (1988) Interaction of hydrogen with solid surfaces. *Surf. Sci. Rep.* **9** 1-163.

[12] Borchers, C., Michler, T. and Pundt, A. (2008) Effect of hydrogen on the mechanical properties of stainless steels. *Adv. Eng. Mater.* **10**(1-2) 11-23.

[13] Langley, R. A. (1984) Hydrogen trapping, diffusion and recombination in austenitic stainless steels. *J. Nucl. Mater.* **128** 622-628.

[14] Şahin, S. and Ubeyli, M. (2008) A Review on the Potential Use of Austenitic Stainless Steels in Nuclear Fusion Reactors. *J. Fusion Energy*. **27** 271–277.

[15] Zinkle, S. J. and J.T., B. (2009) Structural materials for fission & fusion energy. *Mater. Today*. **12** 12-19.

[16] Anoop, M. B., Rao, K. B. and Lakshmanan, N. (2008) Safety assessment of austenitic steel nuclear power plant pipelines against stress corrosion cracking in the presence of hybrid uncertainties. *Int. J. Pres. Ves. Pip.* **85**(4) 238-247.

[17] Scott, C., Allain, S., Faral, M. and Guelton, N. (2006) The development of a new Fe-Mn-C austenitic steel for automotive applications. *Metall. Res. Technol.* **103**(6) 293-302.

[18] Koyama, M., Akiyama, E. and Tsuzaki, K. (2012) Hydrogen embrittlement in a Fe–Mn–C ternary twinning-induced plasticity steel. *Corros. Sci.* **54** 1-4.

[19] Liu, Q., Zhou, Q., Venezuela, J., Zhang, M. and A., A. (2017) Hydrogen influence on some advanced high-strength steels. *Corros. Sci.* **125** 114-138.

[20] Koyama, M., Akiyama, E., Lee, Y.-K., Raabe, D. and K., T. (2017) Overview of hydrogen embrittlement in high-Mn steels. *Int. J. Hydrog. Energy*. **42** 12706-12723.

[21] Anderson, O. L. (1986) Properties of iron at the Earth's core conditions. *Geophys. J. Int.* **84**(3) 561-579.

[22] Olson, D. L. (1985) Prediction of Austenitic Weld Metal Microstructure and Properties. *Weld. J.* **64** 281s-295s.

[23] Tsong-Pyng, P. and Altstetter, C. J. (1986) Effects of deformation on hydrogen permeation in austenitic stainless steels. *Acta Metall.* **34**(9) 1771-1781.

[24] Juan, A., Moro, L., Brizuela, G. and Pronsato, E. (2002) The electronic structure and bonding of an hydrogen pair near a FCC Fe stacking fault. . *Int. J. Hydrogen Energy*. **27**(3) 333-338.

[25] Du, Y. A., Ismer, L., Rogal, J., Hickel, T., Neugebauer, J. and Drautz, R. (2011) First-principles study on the interaction of H interstitials with grain boundaries in α- and γ-Fe. *Phys. Rev. B*. **84**(14) 144121(1)-144121(13).

[26] Grabke, H. J. and Riecke, E. (2000) Absorption and diffusion of hydrogen in steels. *Mater. Tehnol.* **34**(6) 331-342.

[27] Jiang, D. E. and Carter, E. A. (2003) Adsorption and diffusion energetics of hydrogen atoms on Fe(110) from first principles. *Surf. Sci.* **547**(1) 85-98.

[28] Jiang, D. E. and Carter, E. A. (2004) Diffusion of interstitial hydrogen into and through bcc Fe from first principles. *Phys. Rev. B*. **70**(6) 064102(1)-064102(9).

[29] Kimizuka, H., Mori, H. and Ogata, S. (2008) Effect of temperature on fast hydrogen diffusion in iron: A path-integral quantum dynamics approach. *Phys. Rev. B*. **83** 094110(1)-094110(7).

[30] Sanchez, J., Fullea, J., Andrade, C. and de Andres, P. L. (2008) Hydrogen in α-iron: Stress and diffusion. *Phys. Rev. B*. **78** 014113(1)-014113(7).

[31] Kiuchi, K. and McLellan, R. B. (1983) The solubility and diffusivity of hydrogen in well-annealed and deformed iron. *Acta Metall.* **31** 961-984.

[32] Mudiyanselage, K., Yang, Y., Hoffmann, F. M., Furlong, O. J., Hrbek, J., White, M. G., Liu, P. and D.J., S. (2013) Adsorption of hydrogen on the surface and sub-surface of Cu(111). *J. Chem. Phys.* **139** 044712(1)- 044712(8).

[33] Shen, X., Chen, J., Sun, Y. M. and Liang, T. (2016) Hydrogen diffusion on Fe surface and into subsurface from first principles. *Surf. Sci.* **654** 48–55.

[34] Shen, X., Li, Y., Liu, X., Zhang, D. and Gao, J. L. T. (2017) Hydrogen diffusion into the subsurfaces of model metal catalysts from first principles. *Phys. Chem. Chem. Phys.* **19** 3557-3564.

[35] Sholl, D. S. (2007) Using density functional theory to study hydrogen diffusion in metals: A brief overview. *J. Alloys Compd.* **446** 462-468.

[36] Luntz, A. C. (2009) The dynamics of dissociative adsorption on metal surfaces: ‘‘First principles” theory – Experiment confrontations. *Surf. Sci.* **603** 1557–1563.

[37] Kresse, G. and Furthmüller, J. (1996) Efficiency of ab-initio total energy calculations for metals and semiconductors using a plane-wave basis set. *Comp. Mater. Sci.* **6**(1) 15-50.

[38] Perdew, J. P., Burke, K. and Ernzerhof, M. (1996) Generalized Gradient Approximation Made Simple. *Phys. Rev. Lett.* **77**(18) 3865-3868.

[39] Blöchl, P. E. (1994) Projector augmented-wave method. *Phys. Rev. B*. **50**(24) 17953-17979.

[40] Ismer, L., Hickel, T. and Neugebauer, J. (2010) Ab initio study of the solubility and kinetics of hydrogen in austenitic high Mn steels. *Phys. Rev. B*. **81**(9) 094111(1)- 094111(9).

[41] Medvedeva, N. I., Van Aken, D. and Medvedeva, J. E. (2010) Magnetism in bcc and fcc Fe with carbon and manganese. *J. Phys. Condens. Matter*. **22**(31) 316002(1)-316002(7).

[42] Jiang, D. E. and Carter, E. A. (2003) Carbon dissolution and diffusion in ferrite and austenite from first principles. *Phys. Rev. B*. **67**(21) 214103(1)-214103(11).

[43] Herper, H. C., Hoffmann, E. and Entel, P. (1999) Ab initio full-potential study of the structural and magnetic phase stability of iron. *Phys. Rev. B*. **60**(6) 3839-3848.

[44] Dyson, D. J. and Holmes, B. (1970) Effect of alloying additions on the lattice parameter of austenite. *J. Iron Steel Inst.* **208**(5) 469-474.

[45] Pack, J. D. and Monkhorst, H. J. (1976) Special points for Brillouin-zone integrations. *Phys. Rev. B: Condens. Matter*. **13**(12) 5188-5192.

[46] Methfessel, M. P. A. T. and Paxton, A. T. (1989) High-precision sampling for Brillouin-zone integration in metals. *Phys. Rev. B*. **40**(6) 3616-3621.

[47] Payne, M. C., Teter, M. P., Allan, D. C., Arias, T. A. and Joannopoulos, J. D. (1992) Iterative minimization techniques for ab initio total-energy calculations: molecular dynamics and conjugate gradients. *Rev. Mod. Phys.* **64**(4) 1070-1072.

[48] Dillamore, I. L. and Roberts, W. T. (1965) Preferred orientation in wrought and annealed metals. *Metall. Rev.* **10**(39) 271-380.

[49] Oriani, R. A., Hirth, J. P. and Smialowski, M. (1985) *Hydrogen Degradation of Ferrous Alloys* William Andrew Publishing/Noyes.

[50] Uhlemann, M., Engelmann, H.-J. and Mummert, K. (1995) Influence of plastic deformation on the hydrogen diffusivity and solubility in austenitic Fe- and Ni-basic alloys. *Mater. Corros.* **46** 63-70.

[51] Ningshen, S., Uhlemann, M., Schneider, F. and Khatak, H. S. (2001) Diffusion behaviour of hydrogen in nitrogen containing austenitic alloys. *Corros. Sci.* **43** 2255-2264.

[52] Bacher, J. P., Benvenuti, C., Chiggiato, P., Reinert, M. P., Sgobba, S. and Brass, A. M. (2003) Thermal desorption study of selected austenitic stainless steels. *J. Vac. Sci. Technol*. **21**(1) 167-174.

[53] Bernstein, I. M. (1970) The role of hydrogen in the embrittlement of iron and steel. *Mater. Sci. Eng. R-Rep*. **6**(1) 1-19.

[54] Brass, A. M. and Chêne, J. (2006) Hydrogen uptake in 316L stainless steel: Consequences on the tensile properties. *Corros. Sci.* **48**(10) 3222-3242.

[55] Chen, Y., Santos, D. M. and Sequeira, C. A. (2006) Hydrogen Diffusion in Austenitic Stainless Steels. *Trans. Tech. Publ.* **258** 322-326.

[56] Deng, B. Q., Huang, Q. R., Peng, L. L., Mao, O., Du, J. J., Lu, Z. and Liu, X. Z. (1992) Measurement of hydrogen solubility, diffusivity and permeability in HR-1 stainless steel. *J. Nucl. Mater.* **191** 653-656.

[57] Grant, D. M., Cummings, D. L. and Blackburn, D. A. (1988) Hydrogen in 316 steel—diffusion, permeation and surface reaction. *J. Nucl. Mater.* . **152**(2-3) 139-145.

[58] Kanezaki, T., Narazaki, C., Mine, Y., Matsuoka, S. and Murakami, Y. (2008) Effects of hydrogen on fatigue crack growth behavior of austenitic stainless steels. *Int. J. Hydrogen Energy*. **33**(10) 2604-2619.

[59] Louthan, M. R. and Derrick, R. G. (1975) Hydrogen transport in austenitic stainless steel. *Corros. Sci.* **15**(6-12) 565-577.

[60] Zielinski, A. (1990) Effect of hydrogen on internal friction of some FCC metals. *Acta Mater.* **38**(12) 2573-2582.

[61] Kagan, Y. and Klinger, M. I. (1974) Theory of quantum diffusion of atoms in crystals. *J. Phys. C*. **7**(16) 2791-2807.

[62] Hulett, J. R. (1964) Deviations from the Arrhenius equation. *Q. Rev. Chem. Soc.* **18**(3) 227-242.

[63] Chen, L. Y. and Ying, S. C. (1994) Theory of Surface Diffusion: Crossover from Classical to Quantum Regime. *Phys. Rev. Lett.* **73**(5) 700-703.

[64] Zhu, X. D. (1994) Conduction-Electron Effect in Quantum Tunneling Diffusion of Hydrogen on Metal Surfaces. *Phys. Rev. B*. **50**(15) 11279-11282.

Figures

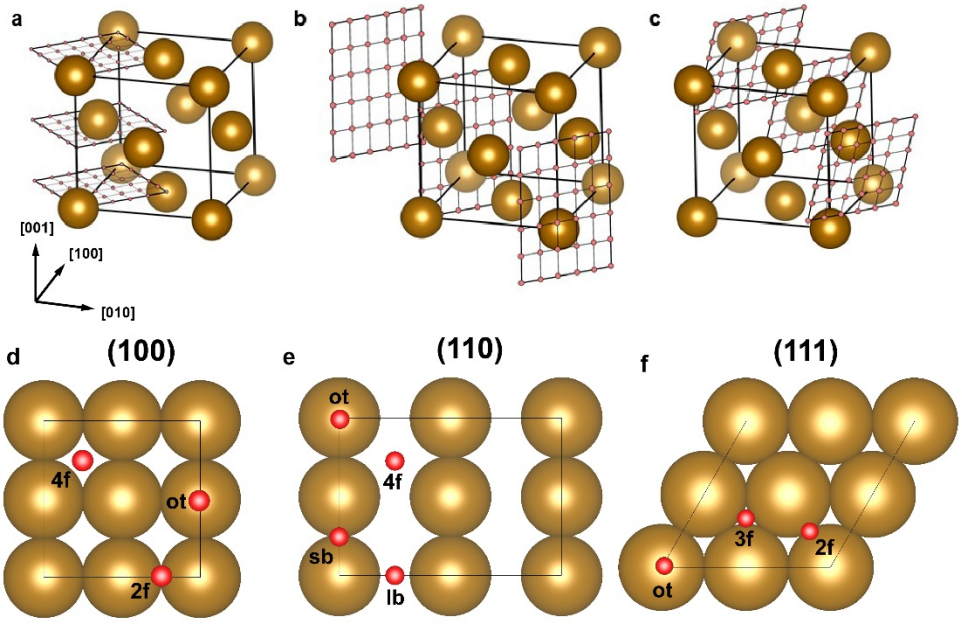

Figure 1: The calculation mesh for the (a) (100), (b) (110), and (c) (111) surfaces. Only three of the nine calculation meshes are displayed for each surface for clarity. The potential adsorption sites are illustrated for the (d) (100), (b) (110), and (c) (111) surfaces. The site notation is as follows: ot = on-top, 2f = two-fold, 3f = three-fold, 4f = four-fold, sb = short-bridge, lb = long-bridge.

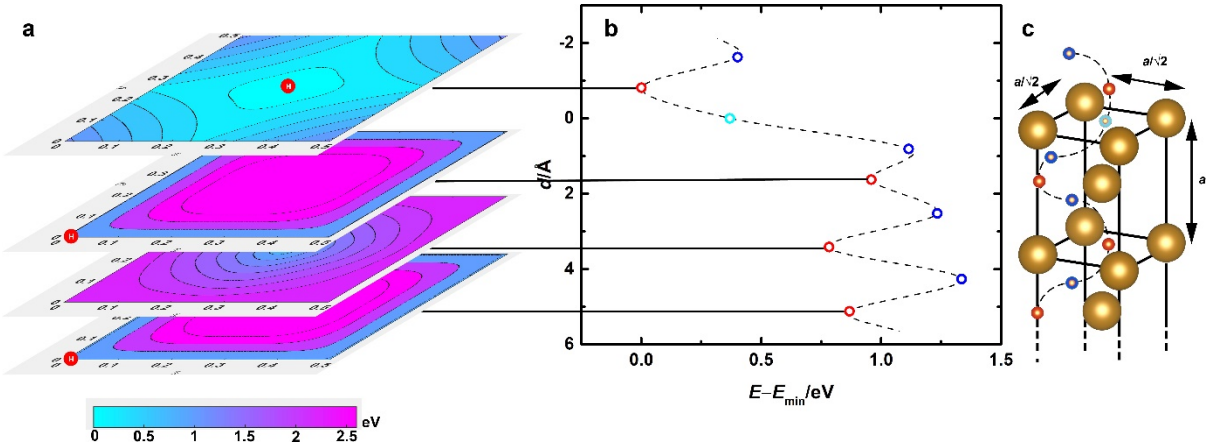

Figure 2: (a) The 2D potential energy surface at local minima for hydrogen diffusion through the (100) surface. (b) The energy profile for hydrogen diffusion through the surface. (c) The diffusion pathway from the surface through towards the bulk. The dotted line between stationary points is only a guide to the eye.

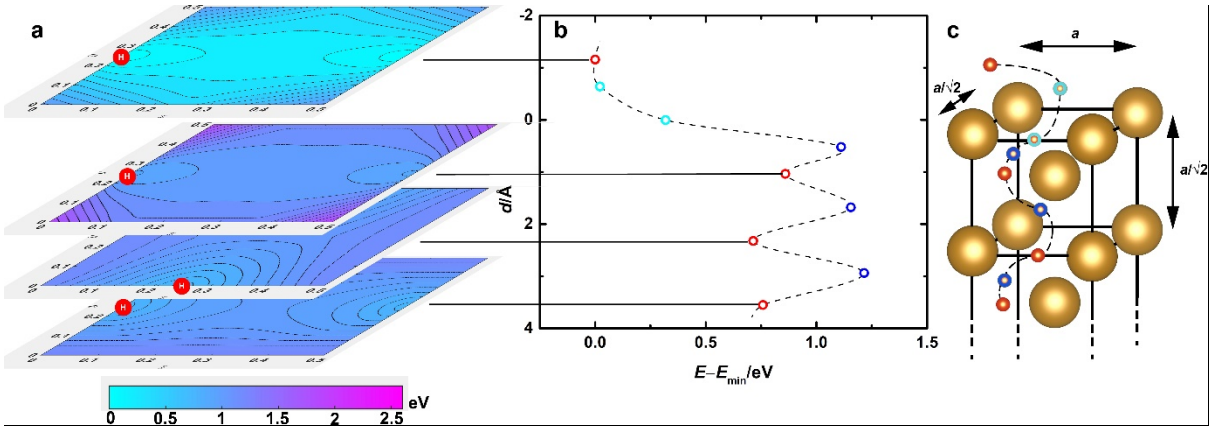

Figure 3: (a) The 2D potential energy surface at local minima for hydrogen diffusion through the (110) surface. (b) The energy profile for hydrogen diffusion through the surface. (c) The diffusion pathway from the surface through towards the bulk. The dotted line between stationary points is only a guide to the eye.

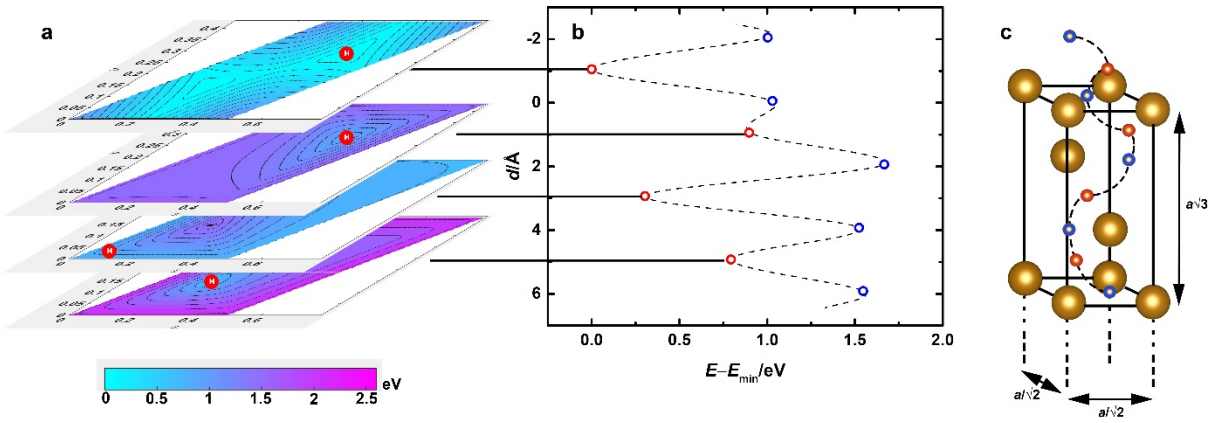

Figure 4: (a) The 2D potential energy surface at local minima for hydrogen diffusion through the (111) surface. (b) The energy profile for hydrogen diffusion through the surface. (c) The diffusion pathway from the surface through towards the bulk. The dotted line between stationary points is only a guide to the eye.

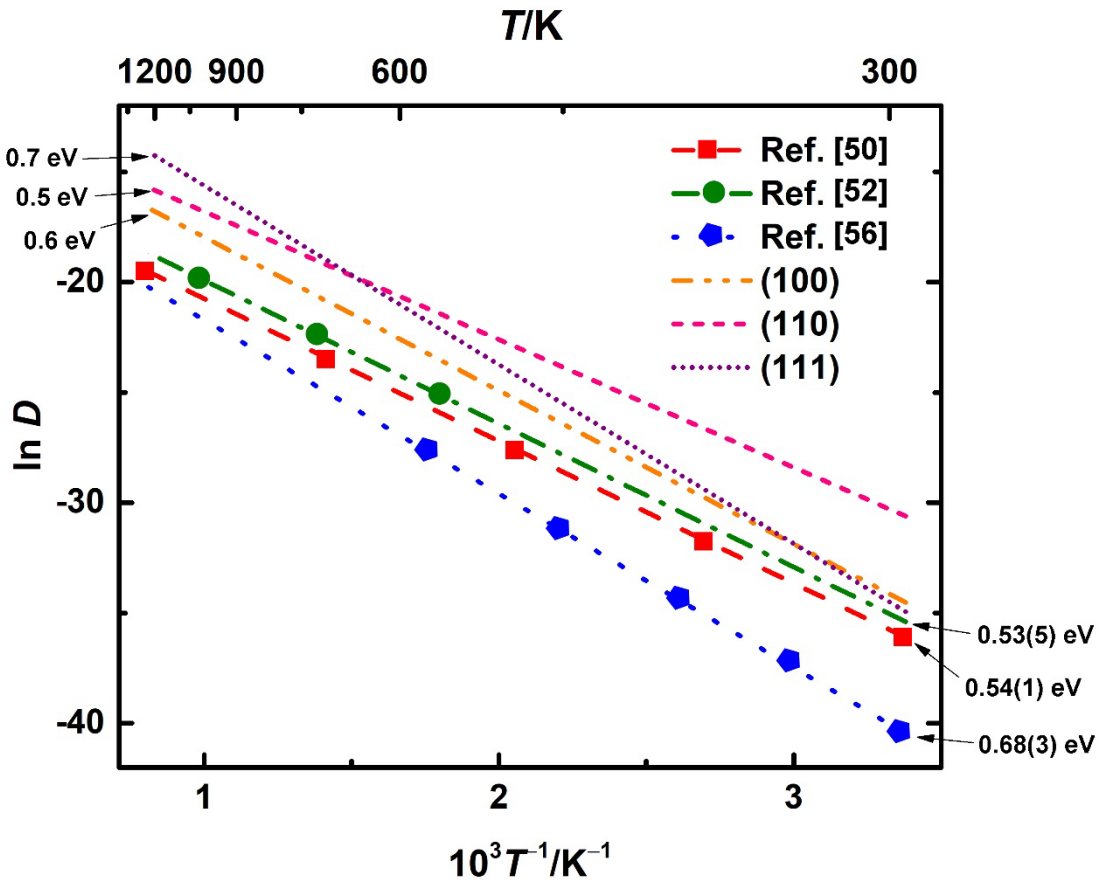

Figure 5: Temperature dependence of the hydrogen diffusion coefficient in γ-Fe, comparing experimental data from literature with the calculations presented in this work for the (100), (110) and (111) surfaces. The activation energy, E_a, is labelled for each dataset. The calculated data has been shifted for clarity.

Tables

Table 1: Relative minimum energies, E-E_{min}, for H in each depth, i, considered in this work for all three γ-Fe surfaces. Each energy is calculated relative to the minimum energy for a particular surface. The preferential adsorption site is indicated in brackets behind the zero values. i = 1,2 are above the surface, i = 3 is at the surface, and i = 4-9 are all below the surface.

Depth index, *i*	**Surface index**		
	(100)	**(110)**	**(111)**
	E-E_{min}/eV		
1	0.40	0.00 (sb)	1.00
2	0.00 (4f)	0.02	0.00 (3f)
3	0.37	0.32	1.00
4	1.12	1.11	0.90
5	0.96	0.86	1.67
6	1.23	1.16	0.30
7	0.78	0.71	1.52
8	1.34	1.22	0.79
9	0.87	0.76	1.55